PHYSICAL REVIEW E **94**, 052113 (2016)

Solvent-mediated forces in critical fluids

Pietro Anzini and Alberto Parola*
Dipartimento di Scienza e Alta Tecnologia, Università dell'Insubria, Via Valleggio 11, 22100 Como, Italy
(Received 11 July 2016; published 7 November 2016)

The effective interaction between two planar walls immersed in a fluid is investigated by use of density functional theory in the supercritical region of the phase diagram. A hard core Yukawa model of fluid is studied with special attention to the critical region. To achieve this goal a formulation of the weighted density approximation coupled with the hierarchical reference theory, able to deal with critical long wavelength fluctuations, is put forward and compared with other approaches. The effective interaction between the walls is seen to change character on lowering the temperature: The strong oscillations induced by layering of the molecules, typical of the depletion mechanism in hard core systems, are gradually smoothed and, close to the critical point, a long range attractive tail emerges leading to a scaling form which agrees with the expectations based on the critical Casimir effect. Strong corrections to scaling are seen to affect the results up to very small reduced temperatures. By use of the Derjaguin approximation, this investigation has natural implications for the aggregation of colloidal particles in critical solvents.

DOI: 10.1103/PhysRevE.94.052113

I. INTRODUCTION

The concept of solvent-mediated interaction among colloidal particles provides an invaluable tool for the physical understanding of the behavior of complex fluids. When two hard nanoparticles are immersed in a molecular solvent, the simple excluded volume constraint is enough to cause an effective attraction between them driven by purely entropic effects, as shown in the seminal work by Asakura and Oosawa (AO) [1,2]. The depletion mechanism has been extensively studied, mostly in hard sphere fluids [3,4], and represents a very successful paradigm for the interpretation of colloidal aggregation. According to the AO prediction, which neglects correlations, the strength of attraction is proportional to the fluid density and its range coincides with the diameter of the solvent molecules. However, both numerical simulations and liquid state theories proved that the effective interaction acquires a remarkable structure when the density of solvent molecules is increased, due to the presence of coordination shells in liquids. Attractive interactions between solvent molecules reduce particle accumulation near the walls giving rise to smoother solvent-mediated forces [5]. In the neighborhoods of the critical point of the fluid the critical Casimir effect [6] is expected to give rise to long range tails in the solvent-mediated attraction between colloidal particles: The effective force between two bodies acquires the range of the correlation length of the underlying critical solvent and is described by a universal scaling law which depends on a very limited number of features (e.g., the geometry of the bodies, the boundary conditions at the colloidal surfaces, the system dimensionality). This remarkable phenomenon has been indeed experimentally observed by use of advanced optical techniques in a lutidine solvent close to its critical point [7]. Numerical simulations have been performed for two representative models of solvent: a square-well fluid and a fluid of hard spheres with three attractive patches. In both cases the emergence of a long range attractive tail in the effective interaction between two large spheres immersed in the solvent is clearly visible [8,9]. An enhanced rate of aggregation among colloidal particles is expected to occur as a result of critical Casimir effect, and indeed also this consequence has been directly observed experimentally [10,11]. These investigations suggest a novel way to control colloidal aggregation by tuning the solvent temperature.

The critical Casimir effect is due to the confinement of order parameter fluctuations induced by the presence of external boundaries. As such, it governs the long range properties of the effective interaction, while at short range excluded volume effects are still present, providing the essential ingredient for the occurrence of the depletion phenomenon. The interplay between these two quite different physical mechanisms which act at different length scales has not been deeply investigated. Numerical simulations showed that, on approaching the critical point, the effective force indeed loses the short range oscillations due to the liquid layering near the surface of the bodies and acquires a smooth attractive form [8,9] but no theoretical study of this effect has been attempted yet. More generally, a thorough investigation of the form of solvent-mediated interactions in the whole phase diagram of a correlated fluid has not been performed. Such a study would clarify the emergence of the long range tails in the effective interactions on approaching the critical region, as well as the coexistence of the depletion mechanism, acting at short distances, and the critical Casimir effect, governing the physics at large distances.

In this paper we tackle this problem by examining the solvent-mediated forces between two hard walls immersed in a hard core Yukawa fluid. The theoretical investigation is performed in the supercritical region in order to exclude wetting phenomena, which deserve a separate analysis. Preliminarily, we must choose the most appropriate theoretical tool for such a study: A natural choice is density functional theory (DFT), which proved accurate in the description of confined fluids. However, no specific implementation of DFT has been investigated in the critical region and most of the liquid state theories, which provide the theoretical basis for the practical formulation of DFT, give a poor description of the critical

*Corresponding author: alberto.parola@uninsubria.it

regime. In Sec. II we propose a weighted density approximation (WDA) especially designed for being accurate also near the critical point. This theory is validated against other DFT prescriptions as well as available numerical simulations in several noncritical states. In Sec. III this approach is applied to the critical region of a Yukawa fluid: The density profiles and the solvent-mediated force between two walls are determined by numerical minimization of the density functional. The development of long range tails in both the density profile and the effective force is quantitatively investigated, confirming the trends already shown in simulations. In Sec. IV the universal properties of the effective interaction in the critical region are discussed. The emergence of scaling laws is investigated in the critical and precritical regime. We also show that, within our approximate DFT formulation, the critical Casimir scaling function is deeply related to the universal bulk properties of the critical fluid. A simple prescription for the theoretical evaluation of the critical and off-critical Casimir scaling function is compared to the numerical results and to available simulations in Ising systems. Section V offers some final comments and perspectives.

II. DENSITY FUNCTIONAL THEORY

The purpose of this work is the investigation of the solvent-mediated interaction between two planar parallel walls immersed in a classical fluid in a wide range of temperatures and densities, including the critical region. In order to achieve this goal we need an accurate description of the properties of a confined fluid. The most successful theoretical approach to study inhomogeneous systems is density functional theory [12]. Although alternative techniques, like integral equations or scaled particle theory, have been proposed [13], DFT is generally considered to be the most accurate and versatile tool for dealing with inhomogeneous systems and has been applied in several frameworks: from the study of fluids in nanopores, to the structure of the liquid-vapor interface, to the theory of freezing (see, e.g., [14]).

A. Weighted density approximation

According to Mermin's extension [15] of the Hohenberg and Kohn density functional theorem [16], the equilibrium density profile $\rho(\boldsymbol{r})$ of a confined fluid can be found by minimizing a suitably defined density functional $\Omega[n(\boldsymbol{r})]$ at fixed chemical potential μ and temperature T. $\Omega[n(\boldsymbol{r})]$ can be conveniently expressed in terms of the external potential $\phi(\boldsymbol{r})$ and the intrinsic free energy functional $\mathcal{F}[n(\boldsymbol{r})]$ as

$$\Omega[n(\boldsymbol{r})] = \mathcal{F}[n(\boldsymbol{r})] - \int d\boldsymbol{r}\, n(\boldsymbol{r})[\mu - \phi(\boldsymbol{r})]. \tag{1}$$

The intrinsic free energy functional is exactly known only in the ideal gas limit

$$\beta\mathcal{F}^{\mathrm{id}}[n(\boldsymbol{r})] = \int d\boldsymbol{r}\, n(\boldsymbol{r})\{\ln[\Lambda^3 n(\boldsymbol{r})] - 1\} \tag{2}$$

[here $\beta = 1/(\mathrm{k_B}T)$ and Λ is the thermal de Broglie wavelength], while, in an interacting system, it is customary to separate this contribution, splitting $\mathcal{F}[n(\boldsymbol{r})]$ as the sum of the ideal and the excess term $\mathcal{F}^{\mathrm{ex}}[n(\boldsymbol{r})]$:

$$\mathcal{F}[n(\boldsymbol{r})] = \mathcal{F}^{\mathrm{id}}[n(\boldsymbol{r})] + \mathcal{F}^{\mathrm{ex}}[n(\boldsymbol{r})]. \tag{3}$$

Several approximations for the excess part have been proposed over the years for dealing with specific problems. Hard sphere fluids are successfully described by Rosenfeld's fundamental measure theory (FMT) [17,18] also at bulk densities close to the solid transition. Even if the FMT is widely used and it its implementation is straightforward, at least for the planar geometry, Rosenfeld's approximation for the excess free energy holds in principle only for fluids of purely hard particles of any shape. Attractive contributions in the interparticle potential are generally added as a mean field perturbation to the reference hard sphere excess free energy functional. However, such an approach gives only qualitative predictions, particularly in the critical region, because it does not take into account correlations arising from the attractive tail of the potential. Also the weighted density approximations (WDAs) by Tarazona [19] and Curtin and Ashcroft [20], whose predictions of the density profile of the hard sphere fluid are rather accurate, at least at moderate densities, include the effects of an attractive tail in the potential only at the mean field level. Furthermore, approaches based on a truncation of the gradient expansion of the excess free energy functional, such as the square-gradient approximation, can describe only the slowly varying part of the density profile but fail in dealing with the short range structure close to the wall.

In order to describe the microscopic properties of the solvent-mediated forces in the whole phase diagram of a fluid, including the liquid-vapor transition, we need an approximation of the excess free energy functional which, in the uniform limit, provides an accurate description of the homogeneous fluid both in the dense and in the critical regime. Unfortunately such an implementation of DFT has not been devised yet. A WDA-based approximation for the excess free energy functional based on the hierarchical reference theory of fluids [21] will now be introduced.

According to the weighted density approximation, the excess free energy functional is expressed in terms of a weighted density $\bar{n}(\boldsymbol{r})$ as

$$\mathcal{F}^{\mathrm{ex}}[n(\boldsymbol{r})] = \int d\boldsymbol{r}\, n(\boldsymbol{r})\psi^{\mathrm{ex}}(\bar{n}(\boldsymbol{r})), \tag{4}$$

where $\psi^{\mathrm{ex}}(\rho)$ is the excess free energy per particle of the homogeneous system evaluated at bulk density ρ and the weighted density $\bar{n}(\boldsymbol{r})$ is written as a local average of the density profile, in terms of an isotropic weight function $w(r;\hat{n})$:

$$\bar{n}(\boldsymbol{r}) = \int d\boldsymbol{r}' n(\boldsymbol{r}') w(|\boldsymbol{r} - \boldsymbol{r}'|; \hat{n}(\boldsymbol{r})). \tag{5}$$

The weight function can be generally dependent on the local value of an auxiliary reference density $\hat{n}(\boldsymbol{r})$ and has to satisfy the normalization requirement

$$\int d\boldsymbol{r}' w(|\boldsymbol{r} - \boldsymbol{r}'|; \hat{n}(\boldsymbol{r})) = 1, \quad \forall\, \boldsymbol{r}, \tag{6}$$

to ensure that in the homogeneous limit the weighted density coincides with the actual density of the fluid.

In order to get a reliable approximation for the excess free energy functional we have to choose properly the two key

ingredients which characterize our WDA ansatz, namely the homogeneous free energy $\psi^{\rm ex}$ and the weight function $w(r;\hat{n})$. The only available microscopic liquid state theory which is able to account both for noncritical and critical properties of a homogeneous fluid is the hierarchical reference theory (HRT) [21], which will be therefore adopted in this work for the evaluation of the excess free energy ψ^{ex} of the uniform fluid.

Although the general formalism of HRT can be applied to fluids and mixtures with arbitrary pair interactions, quantitative results for specific models require the closure of the exact HRT equations by introducing some approximation. A closure which proved remarkably accurate has been implemented in the case of a hard core Yukawa (HCY) fluid [22], because the resulting HRT equations considerably simplify by use of the known solution of the Ornstein-Zernike equation available for this interaction. The HCY potential is defined as the sum of a pure hard core term of diameter σ and an attractive Yukawa tail of inverse range ζ:

$$v_{\rm Y}(r) = -\epsilon\sigma\,\frac{e^{-\zeta(r-\sigma)}}{r}, \quad r \geqslant \sigma, \tag{7}$$

where the parameter ϵ, which defines the energy scale, is positive. In the following we will investigate this model taking σ and $\epsilon/k_{\rm B}$ as the units of length and temperature, respectively.

Having established the form of our excess functional in the homogeneous limit, we proceed with the explicit definition of $\mathcal{F}^{\rm ex}[n(\boldsymbol{r})]$ for general density profiles. We first focus our attention on the effects of the attractive part of the potential. It is well known that its main contribution to the internal energy is given by the Hartree term: this circumstance has been extensively recognized in the previous treatments, where attractive interactions were included just through such a contribution. We are therefore led to isolate this term in the excess free energy, by writing

$$\mathcal{F}^{\rm ex}[n(\boldsymbol{r})] = \mathcal{F}^{\rm ex}_{\rm R}[n(\boldsymbol{r})] + \mathcal{F}^{\rm ex}_{\rm H}[n(\boldsymbol{r})], \tag{8}$$

where the Hartree contribution is given by

$$\mathcal{F}^{\rm ex}_{\rm H}[n(\boldsymbol{r})] = \frac{1}{2}\int d\boldsymbol{r}' \int d\boldsymbol{r}'' n(\boldsymbol{r}')v_{\rm Y}(|\boldsymbol{r}'-\boldsymbol{r}''|)n(\boldsymbol{r}''), \tag{9}$$

whereas the reference term $\mathcal{F}^{\rm ex}_{\rm R}[n(\boldsymbol{r})]$, defined by Eq. (8), contains both the entropic contribution to the free energy, arising from hard core repulsion, and the correlations induced by the attractive interaction. Our choice is then to use WDA to represent only the entropy-correlation part of the intrinsic free energy functional, retaining the exact description of the Hartree energy:

$$\mathcal{F}^{\rm ex}_{\rm R}[n(\boldsymbol{r})] = \int d\boldsymbol{r}\, n(\boldsymbol{r})\psi^{\rm ex}_{\rm R}(\bar{n}(\boldsymbol{r})), \tag{10}$$

where

$$\psi^{\rm ex}_{\rm R}(\rho) = \psi^{\rm ex}(\rho) - \frac{\rho}{2}\int d\boldsymbol{r}\, v_{\rm Y}(r). \tag{11}$$

The form of the weight function can be determined following the strategy put forward by Tarazona [19], by requiring that the two-particle direct correlation function reduces, in the homogeneous limit, to the known form of the underlying bulk liquid state theory which, in our case, is the direct correlation function $c(r,\rho)$ predicted by HRT:

$$-\beta\frac{\delta^2\mathcal{F}^{\rm ex}_{\rm R}[n]}{\delta n(\boldsymbol{r})\delta n(\boldsymbol{r}')}\bigg|_{n(\boldsymbol{r})=\rho_b} = c(|\boldsymbol{r}-\boldsymbol{r}'|;\rho_b) + \beta\, v_{\rm Y}(|\boldsymbol{r}-\boldsymbol{r}'|) \equiv c_{\rm R}(|\boldsymbol{r}-\boldsymbol{r}'|;\rho_b), \tag{12}$$

where the last equality is a definition. This constraint can be fulfilled only by a density-dependent weight function. In a previous work Curtin and Ashcroft [20] proposed that the weight function should depend on the local value of the weighted density itself, i.e., $\hat{n}(\boldsymbol{r}) = \bar{n}(\boldsymbol{r})$. Unfortunately, even for a purely repulsive hard sphere system, this hypothesis leads to difficulties in the solution of the nonlinear differential equation for the weight function [58] which must be imposed in order to implement the constraint (12). This problem can be overcome choosing a position-independent auxiliary density $\hat{n}(\boldsymbol{r})$, as suggested by Leidl and Wagner [23]. In our application of DFT to the description of confined systems, we assume that the auxiliary density actually coincides with the homogeneous density at the same chemical potential (also referred to as *bulk density*); i.e., we set

$$\hat{n}(\boldsymbol{r}) = \rho_b. \tag{13}$$

It is straightforward to obtain from Eq. (12) an algebraic equation for the Fourier transform of the weight function:

$$\beta\rho_b\frac{\partial^2\psi^{\rm ex}_{\rm R}}{\partial\rho^2}\bigg|_{\rho_b} w^2(q;\rho_b) + 2\beta\frac{\partial\psi^{\rm ex}_{\rm R}}{\partial\rho}\bigg|_{\rho_b} w(q;\rho_b) + c_{\rm R}(q;\rho_b) = 0, \tag{14}$$

which, at least in the cases examined in this work, always admits real solutions. The physical root can be determined enforcing the normalization condition (6), recalling that the compressibility sum rule, satisfied by the HRT direct correlation function, requires

$$c_{\rm R}(0;\rho) = \int d\boldsymbol{r}\, c_{\rm R}(r;\rho) = -2\beta\frac{\partial\psi^{\rm ex}_{\rm R}}{\partial\rho} - \beta\rho\frac{\partial^2\psi^{\rm ex}_{\rm R}}{\partial\rho^2}. \tag{15}$$

As in other implementations of WDA, the range of the weight function always remains comparable to the size of the molecules. This feature is preserved also in the critical region, as shown in Fig. 1.

Once the intrinsic density functional has been determined, the approximate equilibrium properties, such as the density profile $\rho(\boldsymbol{r})$ and the grand canonical potential $\Omega[\rho(\boldsymbol{r})]$, can be obtained minimizing the functional (1) at fixed temperature and chemical potential. In a HCY fluid, the value of the chemical potential is related to the bulk density by

$$\mu = \frac{1}{\beta}\ln\rho_b + \psi^{\rm ex}_{\rm R}(\rho_b) + \rho_b\frac{d\psi^{\rm ex}_{\rm R}}{d\rho}\bigg|_{\rho_b} - 4\pi\frac{\zeta+1}{\zeta^2}\rho_b. \tag{16}$$

A central quantity for the present investigation is the force acting on the two planar hard walls in the HCY fluid. In this geometry, symmetry requires that all the local properties may depend on the single coordinate z, orthogonal to the two plates, placed at $z = 0$ and $z = L$, respectively. Remarkably, if the wall separation h is greater than σ, the force per unit surface f acting on the plates, sometimes called *solvation force*, can

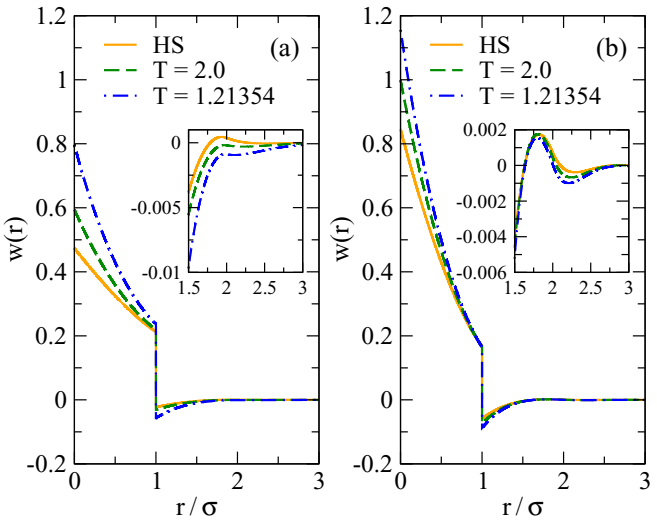

FIG. 1. Real space weight function at two values of bulk density [(a) $\rho_b\sigma^3 = 0.3154$, (b) $\rho_b\sigma^3 = 0.6$] for three values of the temperature. One state shown here ($\rho_b\sigma^3 = 0.3154$, $T = 1.21354$) is very close to the critical point.

be expressed as a pressure difference [24]:

$$f(L;T,\mu) = -\frac{\partial}{\partial L}\left(\frac{\Omega^{(L)}[\rho(z)]}{\Sigma}\right)\Bigg|_{T,\mu} - p_b(T,\mu), \quad (17)$$

where $\Omega^{(L)}[\rho(z)]/\Sigma$ is the grand canonical potential per unit surface of the fluid confined in the region $[0,L]$, determined by the minimization of the approximated grand canonical functional at fixed (μ,T), and $p_b(\mu,T)$ is the pressure of the fluid at the same values of temperature T and chemical potential $\mu = \mu(\rho_b,T)$. On the other hand, when $L < \sigma$ there are no particles between the walls and the attractive force per unit surface acting on the walls arises uniquely from the presence of the fluid in the regions $z < 0$ and $z > L$: The first term in Eq. (17) vanishes and the force is given by

$$f(L;T,\mu) = -p_b(T,\mu). \quad (18)$$

The solvation force f defined above is a difference of pressures and goes to zero in the limit $L \to \infty$. By means of standard functional identities it is possible to express, without any further approximation, the derivative of the grand potential per unit surface in terms of the contact density:

$$\rho_w^{(L)} \equiv \lim_{\delta\to 0^+} \rho(L - \sigma/2 - \delta) = \lim_{\delta\to 0^+} \rho(\sigma/2 + \delta), \quad (19)$$

and the solvation force can be finally written as [25]

$$f(L;T,\mu) = \mathrm{k_B}T\,\rho_w^{(L)} - p_b(T,\mu). \quad (20)$$

We also remark that this version of WDA exactly satisfies the contact value theorem [26]

$$\beta p_b(T,\mu) = \lim_{L\to\infty} \rho_w^{(L)}, \quad (21)$$

leading to the more suggestive identity

$$\beta f(L;T,\mu) = \rho_w^{(L)} - \rho_w^{(\infty)}. \quad (22)$$

The above results show that, in order to obtain the force acting on the walls, we just need to perform the minimization of the functional in the region $[0,L]$ in order to evaluate the contact density $\rho_c^{(L)}$. The minimization has been be carried out by a simple iterative (Picard) method, taking advantage of the exact implicit relation for the approximate equilibrium density profile $\rho(z)$ given by

$$\rho(z) = \exp\left[-\beta(u(z) - \mu)\right], \quad (23)$$

where the potential of mean force $u(z)$ is defined as

$$u(z) = \frac{\delta\mathcal{F}_{\mathrm{R}}^{\mathrm{ex}}[n]}{\delta n(\boldsymbol{r})}\Bigg|_{\rho(z)} + \int d\boldsymbol{r}'\rho(z')v_{\mathrm{Y}}(|\boldsymbol{r} - \boldsymbol{r}'|). \quad (24)$$

A spatial step size $\Delta z = 1.5 \times 10^{-2}\sigma$ has been generally used in the numerical minimization, while for bulk densities $\rho_b\sigma^3 > 0.7$, and close to the critical point Δz has been reduced up to two orders of magnitude. Typically, up to few thousand Picard iterations were necessary to achieve a precision of one part in 10^7 for the density profile and one part in 10^{11} in the grand potential.

B. Validation of the method

The minimization of the previously defined grand canonical functional allows us to evaluate the equilibrium properties of the confined fluid. Within this approach, the relevant quantities can be found at every temperature and bulk density of interest, also in the vicinity and below the critical point of the HCY fluid. Most of the calculations refer to a Yukawa fluid with range $\zeta\sigma = 1.8$, where several simulation results are available. We performed minimizations of the functional for values of the temperature T above the critical point ($T > T_c \sim 1.21353$) and bulk reduced densities $\rho_b\sigma^3$ up to 0.85.

In the high temperature limit our model reduces to a hard sphere fluid, whose properties have been extensively investigated by numerical simulations. Figure 2 shows the density profiles $\rho(z)$ of a hard sphere fluid near a hard wall at two different values of ρ_b. The agreement of the WDA prediction with the Monte Carlo (MC) data of Ref. [27] is very good up to reduced densities of the order of 0.6, while at higher values the phase of oscillations in the density profile is correctly captured, although a slight underestimation of the peak value is observed. The comparison of our density profiles with those predicted by the "White Bear" version of the FMT [28] shows, as expected, that Rosenfeld's theory gives more accurate estimates of the oscillation peaks, particularly at high density.

When the temperature is decreased the contribution of the Yukawa tail to the density profile becomes relevant. We compared the density profile obtained within our DFT approximation with the MC simulation data for $\zeta\sigma = 1.8$ at temperature $T = 2$ and for $\zeta\sigma = 3$ at $T = 1.004$. Figure 3 shows that the WDA estimate is remarkably accurate at reduced densities 0.4 and 0.5; small deviations from the MC simulation data appear at reduced density 0.7. We note that at $\rho_b\sigma^3 = 0.7$ the contact reduced density is overestimated by about 0.2 with respect to simulation data, even if the contact theorem is verified with a relative error of the order of 10^{-5}. This disagreement in the contact value is due to different estimates of the grand canonical potential per unit volume of the homogeneous fluid and it is compatible with the the spread in the values of the bulk pressure obtained within

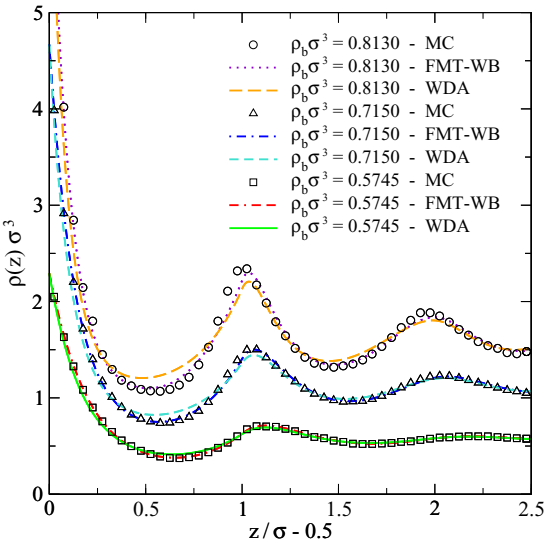

FIG. 2. Density profiles $\rho(z)$ for a hard sphere fluid between two hard walls (distance $L = 16\sigma$) at different values of the bulk reduced density $\rho_b\sigma^3$. MC simulation data (symbols) are taken from Ref. [27]. We have obtained the FMT density profiles (lines) from the minimization of the approximated FMT-WB functional [28]. To enhance visual clarity the density profiles at $\rho_b\sigma^3 = 0.715$ and $\rho_b\sigma^3 = 0.813$ are shifted upward by 0.4 and 0.8, respectively.

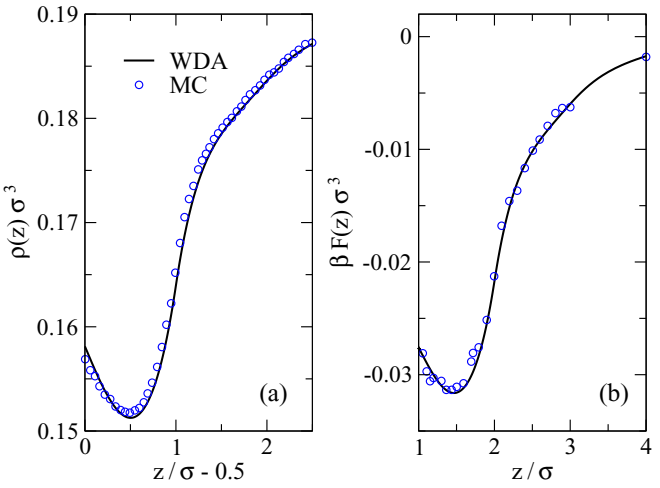

FIG. 4. (a) Density profile $\rho(z)$ of a HCY fluid at a single hard wall ($\zeta\sigma = 3$) for bulk reduced density $\rho_b\sigma^3 = 0.191$ and temperature $T = 1.004$. Lines represent the predictions of the present WDA. Points are MC data from Ref. [32]. (b) Force per unit surface acting between two infinite parallel hard walls immersed in a HCY fluid ($\zeta\sigma = 3$) in the same thermodynamic state as panel (a). Lines are the predictions of the WDA from Eq. (20), whereas points represent the MD simulation of Ref. [32].

different simulation techniques [29]. In panel (a) of Fig. 4 we compare our results for the density profile of the HCY fluid characterized by $\zeta\sigma = 3$ with the recent MC simulations from Ref. [32]. This figure shows that at relatively low densities the agreement between our approximation and MC predictions is remarkable also for attractive potentials of shorter range. In particular we predict accurately the kink in the density profile at $\rho_b\sigma^3 = 0.191$, which is only qualitatively reproduced within mean field approximation [32].

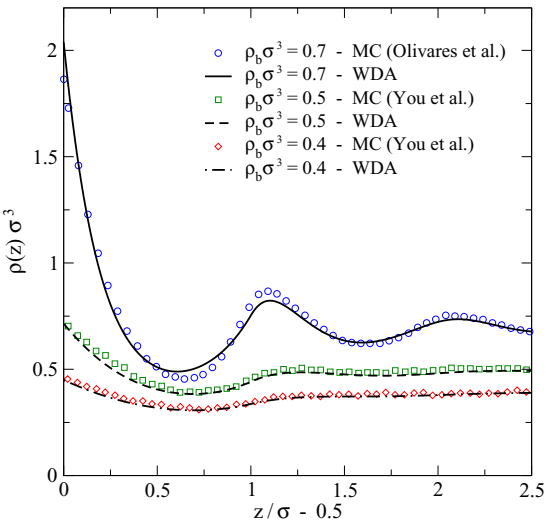

FIG. 3. Density profile $\rho(z)$ of a Yukawa hard sphere fluid ($\zeta\sigma = 1.8$) at reduced temperature $T = 2$ confined between two hard walls at different values of bulk reduced density $\rho_b\sigma^3$. Lines represent the predictions of the present WDA. Points are MC data from Ref. [30] (reduced density 0.7) and Ref. [31] (reduced density 0.4 and 0.5). The distance between the walls is 10σ.

The minimization of the grand canonical functional provides both the value of the contact density $\rho_w^{(L)}$ and of the grand free energy. It is therefore possible to obtain the depletion force either by calculating the derivative with respect to L of the grand potential, as in Eq. (17), or by making use of Eq. (20). The consistency between the two estimates is a good check for the accuracy of the numerical procedure. To give an example, for a hard sphere fluid, the relative difference between the two results is less than 0.01% if the absolute value of the force per unit surface and k_BT is larger than 10^{-6}. Nonetheless at smaller values of the force the result obtained by differentiation of the grand free energy is less stable, due to errors introduced by the discretization.

The solvent-mediated force acting on two parallel hard walls immersed in a hard sphere fluid is compared with the Monte Carlo data of Wertheim *et al.* [33] as well as the predictions based on FMT in Fig. 5, showing a nice agreement also at relatively high densities. At reduced density 0.2873 the force maximum per unit surface is of the order of k_BT/σ^3, and the oscillations due to the packing of the hard spheres are damped within two or three diameters. Furthermore, at this value of the reduced density, a small deviation between WDA and FMT is present only at the first minimum. At reduced density 0.6 the force at distances of the order of the hard sphere diameter σ is a hundred times larger than at $\rho_b\sigma^3 = 0.2873$. Even this feature is well reproduced by both WDA and FMT, as can be seen in the inset. The strong oscillating behavior of the MC data is captured by WDA with a correct phase, even if the peak values are a little underestimated, whereas FMT behaves considerably better.

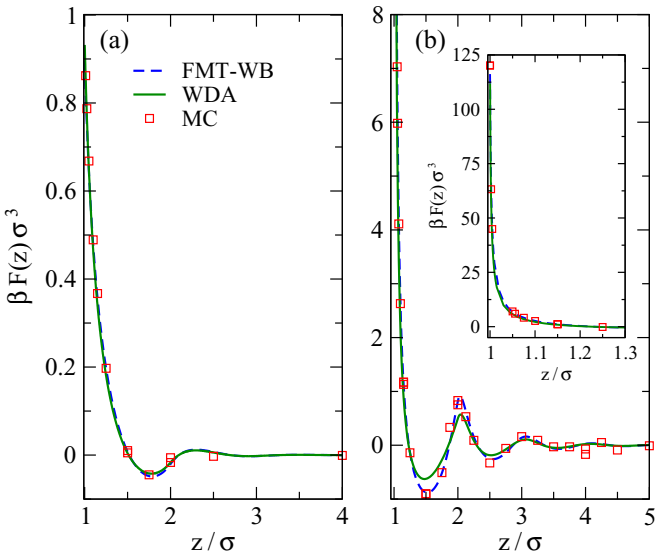

FIG. 5. Force per unit surface and $k_B T$ between two infinite planar hard walls immersed in a fluid of hard spheres of diameter σ for two values of the bulk reduced density: (a) $\rho_b\sigma^3 = 0.2873$, (b) $\rho_b\sigma^3 = 0.6$. The value of the force within the WDA approximation has been obtained via Eq. (20). The FMT-WB result comes from the minimization of the "White Bear" version of the FMT functional [28] via Eq. (20). The MC data are taken from Ref. [33]. The inset highlights the behavior of the force at $\rho_b\sigma^3 = 0.6$ at small distances.

The solvent-mediated force per unit area between two walls in a HCY fluid has not been extensively investigated by numerical simulations. In panel (b) of Fig. 4 we show a comparison between our results and the Monte Carlo data of Ref. [32] for a HCY fluid of inverse range $\zeta\sigma = 3$ at $T = 1.004$ and $\rho_b\sigma^3 = 0.191$. Even if the net force is quite small, our prediction agrees very well with the numerical simulations at all values of the wall separation. We stress that, particularly at small distances, the WDA force is much more accurate than any mean field perturbation method (see Ref. [32]).

The detailed comparisons of our DFT with both numerical simulations and state-of-the-art theories allow us to conclude that in the high temperature limit the present WDA is able to correctly reproduce the density profile and the effective interactions between the hard walls with a very satisfactory accuracy up to reduced densities of about 0.5. Moreover, this formulation of WDA appears to be the best available DFT for a HCY fluid at finite temperature.

III. RESULTS

A. Slab geometry

We performed the minimization of the WDA density functional at several values of temperatures and reduced bulk densities for a HCY fluid of inverse range $\zeta\sigma = 1.8$ confined between two hard walls. At high temperatures the system behaves like a hard sphere fluid, whereas when the temperature is decreased the contribution of the Yukawa tail becomes more and more relevant, and the strongly oscillating character of both the density profiles and the solvent-mediated force is lost.

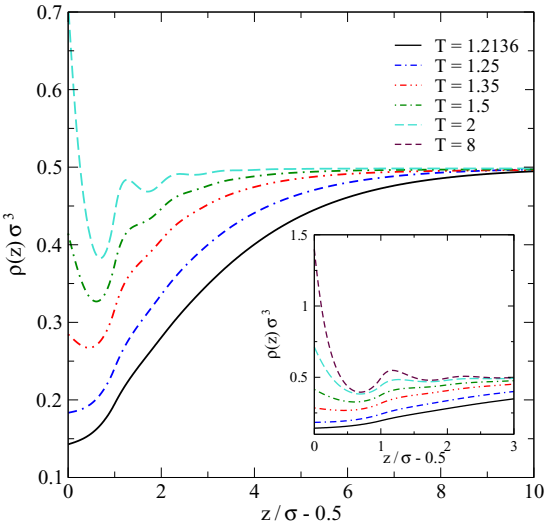

FIG. 6. Density profile of a HCY fluid ($\zeta\sigma = 1.8$) at a single hard wall at bulk reduced density $\rho_b\sigma^3 = 0.5$ and different values of the temperature. The inset shows the same data, also including the density profile at temperature $T = 8$ using a different scale.

Figure 6 shows the dependence of the density profile on temperature at fixed bulk reduced density $\rho_b\sigma^3 = 0.5$. At reduced temperature $T = 8$ the system behaves like a hard sphere fluid. As the temperature is lowered towards its critical value, the density profile gradually becomes monotonic losing the oscillating features typical of hard spheres and the density at contact assumes values four times lower than the bulk density. The range of the perturbation produced by the wall extends at larger and larger distances as the temperature approaches T_c, giving rise to a region where a kind of drying of the wall can be observed.

The attractive tail in the pair interaction of the HCY fluid smoothes the density profile reducing the layering of particles. As a consequence, the effective force between the two walls loses the strongly repulsive peak present at $z \sim \sigma$ when the interaction between the fluid particles is purely hard sphere (see Fig. 5). Figure 7 shows the force per unit surface between the walls for different values of the temperature at the critical bulk reduced density $\rho_c\sigma^3 = 0.3152$. The repulsive contribution to the interaction force, present at $T = 8$, gradually disappears at lower temperatures and the force becomes purely attractive and monotonic, confirming the findings of the numerical simulations in a different model [8]. By approaching the critical temperature ($T_c \sim 1.21353$) the effective force becomes weaker and weaker at short distance, as can be seen in the right panel of Fig. 7: its amplitude reduces almost by a factor of 2 due to a 10% change in temperature. However, a closer look to the long distance tail of the solvent mediated force shows that its range indeed increases close to the critical temperatures, as expected on the basis of scaling arguments. However this occurs at very large separations ($L > 26\sigma$ for the data shown in the figure).

Figure 8 shows the force per unit surface between the walls in different density regimes when the value of the temperature is close to T_c. We note that when the bulk density is higher than ρ_c the force is an order of magnitude larger than for $\rho_b < \rho_c$.

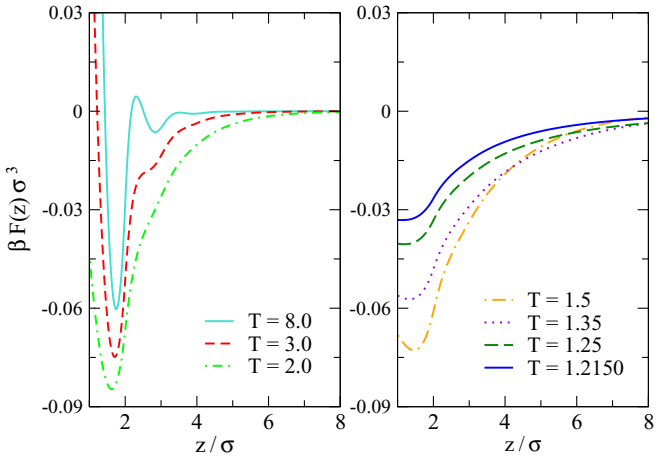

FIG. 7. Force per unit surface acting between two hard walls immersed in a HCY fluid ($\zeta\sigma = 1.8$) obtained from the minimization of the WDA functional using Eq. (20) at $\rho_b\sigma^3 = 0.3152$ and different values of the temperature.

The force is monotonic and purely attractive for all values of the reduced density and its range grows near ρ_c, as expected.

In lattice fluid models the coexistence curve is symmetric about the critical temperature and the critical isochore coincides with the locus $\rho(T)$ of the maxima of the isothermal susceptibility. For such systems, according to the renormalization group terminology, the path to the critical point orthogonal to the relevant odd operator coincides with the critical isochore. In a real fluid the coexistence curve is asymmetric about the critical isochore. In this case a good approximation for the same path is given by the line $\tilde{\rho}(T)$ in the phase diagram defined as the locus of the points (ρ, T) such as

$$\tilde{\rho}(T) = \max_{\rho}\{\rho\,\chi_T\}, \tag{25}$$

where χ_T is the isothermal compressibility.

Figure 9 shows the density profile of the HCY fluid at a hard wall along the line $\tilde{\rho}(T)$. Its behavior at distances larger than the bulk correlation length is well fitted by an exponential of the form

$$\rho(z) = \rho_b + Ae^{-z/\xi}, \tag{26}$$

where ρ_b is the bulk density of the fluid, A is a negative amplitude factor, and ξ is the bulk correlation length. This exponential decay of the density profile is observed also if the system is far from the critical region and is probably related to the location in the bulk phase diagram of the point we investigated with respect to the Fisher-Widom line [34,35].

Following the argument of Ref. [34], we expect that the exponential long range behavior of the density profile reflects an analogous exponential decay of the force between the two walls. Provided we do not cross the Fisher-Widom line, this decay should be present both far from the critical point and in the critical region, where it agrees with the predictions of the theory of the critical Casimir effect [36]:

$$\beta f(z) = f_0 e^{-z/\xi}. \tag{27}$$

The exponential decay of the solvation force is indeed confirmed by the exact solution of a two-dimensional [37] Ising slab under symmetry breaking boundary conditions and was observed in Monte Carlo simulations of three-dimensional simple fluids [8,9]. Figure 10 shows the long distance exponential decay of the force per unit surface and $k_B T$ between two planar hard walls mediated by a HCY

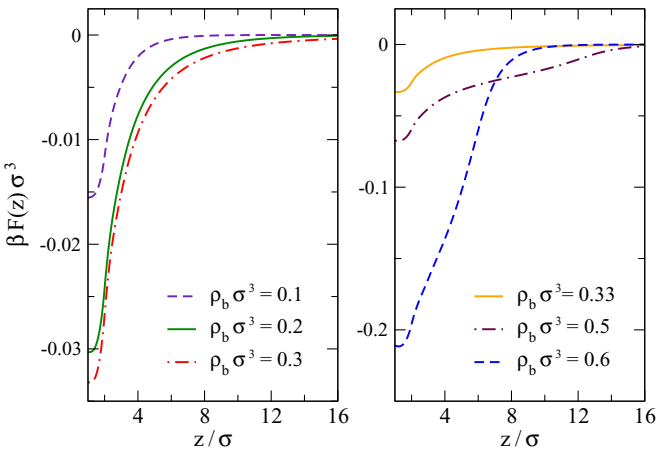

FIG. 8. Force per unit surface acting between two hard walls immersed in a HCY fluid ($\zeta\sigma = 1.8$) obtained from the minimization of the WDA functional using Eq. (20) at $T = 1.2155$ and different values of the reduced density.

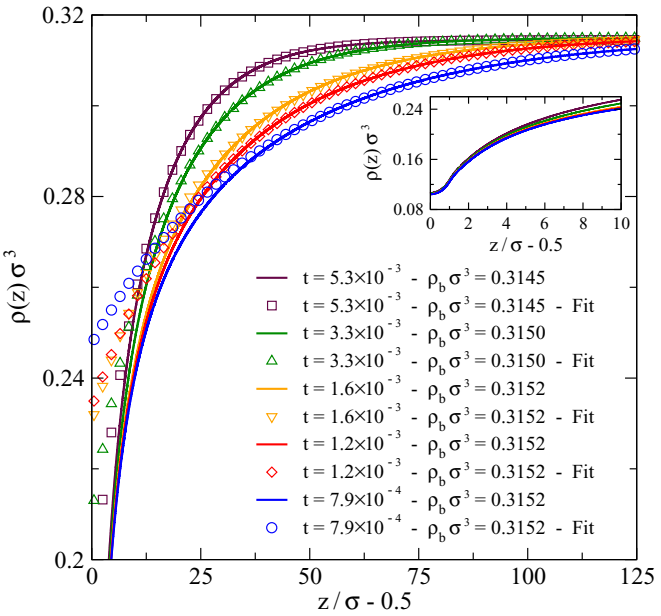

FIG. 9. Lines: Density profile of a HCY fluid ($\zeta\sigma = 1.8$) at a single hard wall in the critical region. Here $t = (T - T_c)/T_c$. Points: Fits of the density profiles according to Eq. (26) performed at distances larger than three times the correlation length of the homogeneous HCY fluid at the same temperature and bulk density. ρ_b, A, and ξ are free fitting parameters and the results obtained for ρ_b and ξ agree well with the bulk values of density and correlation length, respectively (the accuracy is better than 1% for the bulk density and 5% for the correlation length). The bulk correlation lengths obtained from the fitting procedure are $\xi = 41.1\sigma, 31.8\sigma, 26.5\sigma, 17.3\sigma, 12.9\sigma$, from the lowest to the highest reduced temperature. The inset shows a magnification of the same density profiles at short distances.

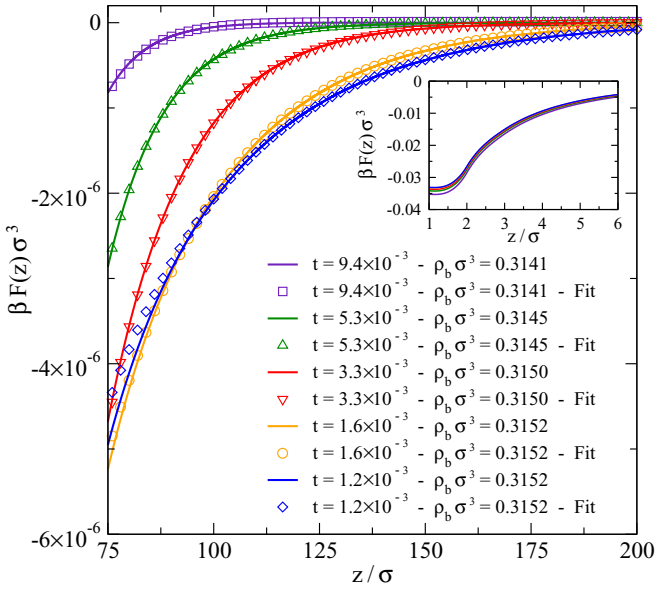

FIG. 10. Lines: Force per unit surface of a HCY fluid ($\zeta\sigma = 1.8$) at a single hard wall along the line $\tilde{\rho}(T)$. Here $t = (T - T_c)/T_c$. Points: Fits of the force according to Eq. (27) performed at distances larger than four times the bulk correlation length of the homogeneous HCY fluid at the same temperature and bulk reduced density. f_0 and ξ are free parameters in the fitting procedure. The result obtained for ξ agrees well with the bulk value of the correlation length (the accuracy of the fit is better than 3%). The bulk correlation lengths obtained from the fitting procedure are $\xi = 31.8\sigma, 26.5\sigma, 17.3\sigma, 12.9\sigma, 9.2\sigma$, from the lowest to the highest reduced temperature. The inset shows the force profile at short distance.

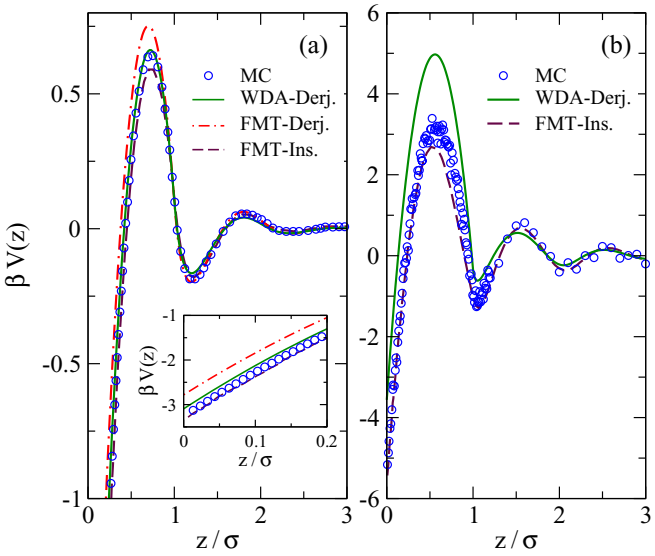

FIG. 11. Depletion potential per unit $k_B T$ between two hard spheres in a fluid of smaller hard spheres (size ratio $q = 0.1$) at bulk packing fraction $\eta = \frac{\pi}{6}\rho_b \sigma^3$ equal to 0.2 (a) and 0.35 (b). MC (points) and FMT predictions obtained with the insertion trick (purple lines) are taken from Ref. [4]. The red line at $\eta = 0.2$ is obtained by use of Derjaguin approximation starting from the solvation force between two planar hard walls evaluated from the FMT-WB [28] approximation. The green lines represent the depletion force obtained within the Derjaguin approximation when the solvation force between the walls is given by the present WDA approximation.

fluid along the critical line $\tilde{\rho}(T)$. The force obtained with our approach is very well fitted by Eq. (27) at large distances $[z \gg \xi(\rho_b, T)]$, whereas at short distances, where depletion effects become relevant, the solvent-mediated force, always attractive, displays a plateau (see inset).

B. Effective interaction between spherical particles

The same WDA formalism previously introduced may be generalized to other interesting geometries, in addition to the planar one. Most importantly, it can be used to evaluate the effective interaction between two spherical particles in a solvent, with obvious applications to the study of aggregation in colloidal suspensions.

The direct minimization of the DFT, although numerically feasible, represents a task considerably more complex than in planar geometry. Therefore, in this first application of the formalism, we have chosen to resort to the simple but effective Derjaguin approximation [38], which allows us to express the interaction between two convex objects starting from the knowledge of the force between two planar walls, independently of the physical origin of the force. According to this approximation, the force F_D between two spheres of radius R can be written as

$$F_D(L) = \pi R \int_L^{+\infty} dz f(z), \tag{28}$$

where L is the minimal surface-to-surface distance between the sphere and $f(z)$ is the force per unit surface between the two walls at distance z. This approximation gives accurate results provided $L \ll R$ and if the interaction potential between the two walls decays rapidly at large distances.

When the force between the walls is mediated by a hard sphere fluid with particles of diameter σ it is possible to show that Derjaguin's expression is the best approximation of the true depletion interaction without taking in account curvature effects [39] and it is accurate in the limit of $q \ll 1$, where $q = \sigma/2R$ is the size ratio. The limits of the Derjaguin approximation when applied to depletion interactions is a debated issue. Particularly, it is a matter of discussion the size ratio at which Derjaguin's theory starts to fail, and how its accuracy depends on the concentration of depletant. In Fig. 11 we compare the prediction for the depletion potential $\beta V(L)$ between two big hard spheres in a fluid of smaller hard spheres obtained both by the Derjaguin approximation and MC simulations at two different values of the bulk density of the smaller particles. The predictions for the depletion potential obtained by the Derjaguin approximation are accurate at $q = 0.1$ only at values of the packing fraction of the small spheres lower than 0.25. At $\eta = 0.35$ the Derjaguin approximation overestimates by about $2k_B T$ both the contact value and the first repulsive peak in the potential, while the oscillations at larger values of distance are underestimated when compared to MC data. The rather poor performance of the Derjaguin approximation is probably due to the presence of a strong repulsive peak in the solvation force between the two walls

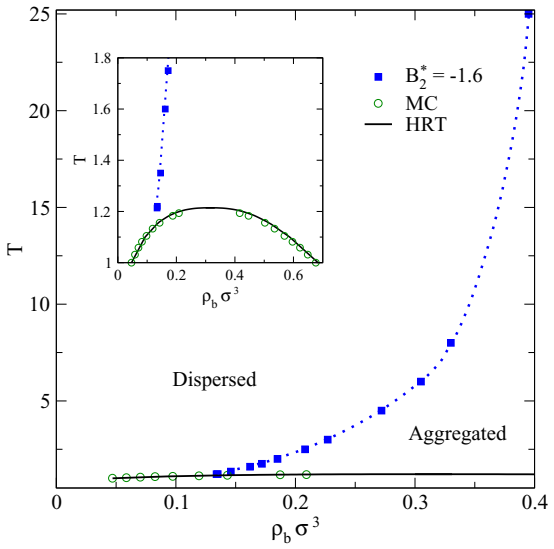

FIG. 12. Phase diagram of the HCY model ($\zeta\sigma = 1.8$) in the (ρ_b, T) plane. The HRT results for the coexistence curve [22] are shown by a black line. Green dots represent the MC data from Ref. [42]. Blue points show the aggregation boundary of two big hard spheres [size ratio $q = \sigma/(2R) = 0.1$] predicted on the basis of our WDA plus Derjaguin approximation and Noro-Frenkel criterion. The dashed line connecting the points is a guide to the eye: aggregation takes place on the right of this boundary. The inset shows the same phase diagram in a wider density interval.

at $z \sim \sigma$ (see Fig. 5) which appears to be a peculiarity of the slab geometry. We expect that, for smoother interwall effective interactions, the agreement would be considerably better.

The results presented above show that the Derjaguin approximation can be safely adopted if the size ratio between the depletant and the colloid is sufficiently small and up to moderate densities of depletant (i.e., $q < 0.1$ and $\rho_b\sigma^3 < 0.4$), and we expect that similar considerations apply when the depletant is a Yukawa hard core fluid. Within the limits of validity of the Derjaguin approximation, we can determine the solvent-mediated potential $v_{\rm eff}(r)$ between two hard spheres of radius R immersed in a HCY fluid in order to examine the phase stability of such a colloidal suspension.

According to Noro-Frenkel extended law of corresponding states [40], fluids characterized by short ranged interaction potentials obey the same equation of state, when expressed in terms of reduced variables. In particular, it was observed that the dimensionless second virial coefficient

$$B_2^*(T) = \frac{B_2(T)}{B_2^{\rm HS}} = 1 + \frac{3}{8R^3}\int_{2R}^{\infty} dr\, r^2 (1 - e^{-\beta v_{\rm eff}(r)}), \quad (29)$$

where $B_2^{\rm HS}$ is the second virial coefficient of a hard sphere system with particles of radius R, assumes a value of about -1.6 at the critical point independently on the particular form of the interaction and that its value remains constant in a relatively large density range across the critical point [41]. It is therefore possible to estimate the gas-liquid spinodal line for a system of hard sphere colloidal particles dispersed in a HCY fluid, by evaluating their reduced second virial coefficient. The blue points in Fig. 12 identify the phase separation line of a HS fluid induced by the presence of a depletant modeled as a HCY fluid. The size ratio between the depletant and the guest HS particles is $q = 0.1$. At high values of the reduced temperature the phase separation occurs at reduced density of about 0.4, as expected in the limit of HS depletant. When the temperature decreases, the concentration of depletant needed to induce phase separation decreases monotonically. At the depletant critical temperature we observe phase separation at depletant concentrations $\rho_b\sigma^3 \sim 0.15$ much lower than the critical one. This implies that at this value of the size ratio q, the phase separation is not related to the presence of long range tails in the effective force, which characterizes the critical region of the solvent, but is still mainly due to the short range attraction generated by the depletion mechanism.

We note that whenever a direct short range repulsion is present between the colloidal particles, as for the case of charged systems, the strong attraction due to depletion is severely weakened and particle aggregation takes place at considerably larger solvent densities. Instead, in the critical region, the long range tails of the solvent-mediated (Casimir) force is not effectively contrasted by the additional short range repulsion. In extreme circumstances (i.e., when the direct repulsion between particles is sufficiently strong), ordinary depletion may be fully screened and phase separation inhibited. However, aggregation is generally expected in a small pocket within the critical region, due to the emergence of long range Casimir forces. For repulsive wall-solvent interactions, this pocket will be centered at solvent densities larger than the critical one, due to the strong asymmetry of the critical Casimir forces (see, e.g., Figs. 8 and 14).

IV. CRITICAL CASIMIR EFFECT

A. Force profiles

The aim of this section is to evaluate the solvent-mediated interaction induced between two walls when the depletant is in the critical regime. Thermal fluctuations in fluids occur on a characteristic range, determined by the correlation length ξ, which usually is comparable with the molecular diameter or with the range of the interactions. When approaching a second-order phase transition, the range of the fluctuations of the order parameter (the particle density in the case of a simple fluid) grows larger up to diverging at the critical point. In this regime the effective force between two bodies immersed in the critical fluid acquires a universal form and obeys scaling laws, as many physical properties near criticality do.

In 1978 [6] Fisher and de Gennes first recognized that a confinement of the critical fluctuations of the order parameter gives rise to an universal long-ranged fluctuation-induced interaction which they named the critical Casimir force. According to the finite-size scaling approach, the universal contribution to the force per unit surface F_C acting between two infinite plates confining a critical fluid can be written as [43,44]

$$\frac{F_C(L;t,h)}{k_B T} = \frac{1}{L^3}\Theta(\pm s, \pm y), \quad (30)$$

where L is the distance between the two walls. The upper sign refers to the supercritical temperature (while the lower to the

subcritical one) and the scaling variables (s,y)

$$s \equiv \frac{L}{\xi}, \quad y \equiv ah|t|^{-\beta\delta} \tag{31}$$

are defined in terms of the two scaling fields

$$t = \frac{T - T_c}{T_c}, \quad h = \mu - \mu_c. \tag{32}$$

Here $\xi \sim \xi_0^{\pm} t^{-\nu}$ is the bulk correlation length at $h = 0$, a is a nonuniversal metric factor, and ν, β, and δ are the usual critical exponents. The function $\Theta(\cdot,\cdot)$ is usually referred to as the scaling function of the critical Casimir force in planar geometry. This function is universal in the sense that it depends only on the bulk universality class, on the boundary conditions imposed at the confining surfaces, and on the geometry of the system (which in this case is $\infty^2 \times L$). We remark that there is no extra metric factor associated with L/ξ and that there is a dependence on the sign of the field h because boundary conditions at the walls break the bulk symmetry $h \to -h$. According to the theory of finite-size scaling, Eq. (30) represents the asymptotic decay of the solvent-mediated force as $t,h \to 0$ and for $L,\xi \to \infty$.

The bulk Yukawa fluid under investigation belongs to the 3D Ising universality class and the boundary conditions are determined by the affinity of the wall surfaces with the fluid particles: if the contact density is less than the bulk density the boundary condition is of type $-$, otherwise of type $+$. In this work we only deal with supercritical temperatures ($t > 0$) and with symmetric $(-,-)$ boundary conditions, which arise for purely repulsive interactions between the fluid particles and two identical confining hard walls.

The analysis of the critical Casimir force and of the related universal scaling function Θ is a rather difficult task both experimentally, for the small forces involved, and theoretically, for the lack of an accurate description of critical fluids in confined geometries. Most of the results present in the literature deal with the temperature dependence of the Casimir fluctuation induced interaction at zero magnetic field. An indirect estimate of the scaling function for the film geometry and the 3D Ising universality class, at $h = 0$ under $(+,-)$ and $(+,+)$ boundary conditions, was given in Ref. [45,46] monitoring the thickness of a binary fluid film at different temperatures near T_c. The first direct evaluation of the critical Casimir force was performed in 2008 [7] for a system consisting of a colloidal particle close to a wall immersed in a binary mixture (sphere-plate geometry) of water and lutidine at different compositions and for both the relevant boundary conditions. This experiment, however, allowed one to probe only the exponential tail of the scaling function. A MC study of the solvent-mediated potential between two spherical particles in a simple fluid along the critical isochore has been performed in Refs. [8,9] with different boundary conditions. However, the determination of the full Casimir scaling function could not be obtained in the temperature range examined in the simulations. Along the symmetry line ($h = 0$), more precise estimates of the universal Casimir scaling functions for the 3D Ising universality class and film geometry have been obtained via MC simulations of the Ising model [47–49]. A few theoretical approaches were devised to address this problem: in addition to the mean field results [50], its is worthwhile mentioning the extended de Gennes–Fisher local functional method [51,52] and a long wavelength analysis of density functional theory [10,53]. The latter investigations have been also extended away from the symmetry line ($h \neq 0$) providing predictions on the shape of the critical Casimir scaling function in the off-critical case [53–55]. Monte Carlo simulations at $h \neq 0$ were recently performed in Ref. [56].

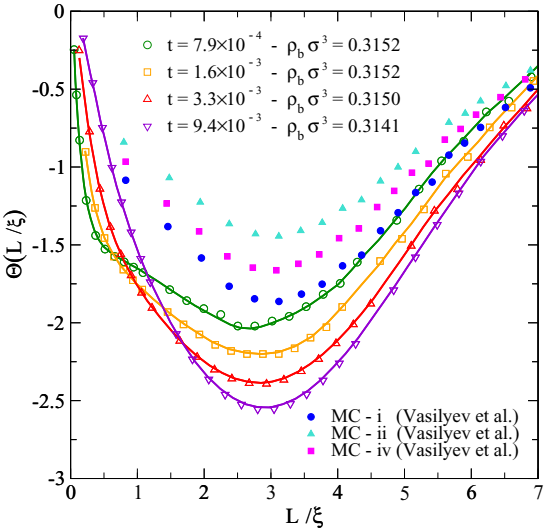

FIG. 13. Finite-size estimates of the Casimir scaling function at values of temperatures and density along the critical line defined in Eq. (25) from the microscopic force obtained within the present WDA approximation. The corresponding bulk correlation lengths are $\xi = 41.1\sigma, 26.5\sigma, 17.3\sigma, 9.2\sigma$, from the lowest to the highest reduced temperature. The lines connecting the points are a guide to the eye. The MC data are taken from Ref. [48] and refer to $(-,-)$ boundary conditions and the different sets correspond to different estimates of the corrections to scaling.

The WDA approach developed above allows the study of this problem starting from the microscopic HCY fluid model confined between two walls. According to the scaling hypothesis, the effective force per unit surface between the two walls F_C should depend on the physical control parameters T,μ,L only through the combination (30), implying the collapse of different data sets onto the same universal curve. Figure 13 shows the scaling function obtained from independent calculations at different temperatures along the previously defined critical line $\tilde{\rho}(t)$ (i.e., $y = 0$). Note that, even at reduced temperature $t = (T - T_c)/T_c$ as low as 10^{-3}, our estimates show a marked temperature dependence, and the data along different isotherms do not collapse as we expected. At the lowest temperature we investigated, a significant difference between our prediction and the MC simulations of Ref. [48] suggests the presence of strong corrections to scaling. We also remark that the curves at the lowest temperatures develop a kink at small values of L/ξ, due to the singular behavior of the scaling function at $L/\xi = 0$. In fact, at any given reduced temperature $t \neq 0$, the quantity $L^3 F_C$ tends to zero as $L/\xi \to 0$, forcing the finite-size estimate of the scaling function to vanish. Figure 14 shows the scaling function at fixed temperature near T_c for different values of the scaling variable $y = ah|t|^{-\beta\delta}$, corresponding to different bulk reduced

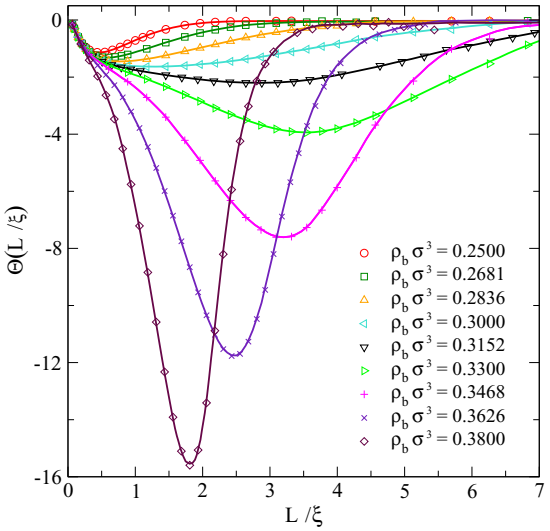

FIG. 14. Scaling function for the critical Casimir force at $t = 1.6 \times 10^{-3}$ and for different values of the scaling variable y. The lines connecting the points are a guide to the eye. The largest correlation length, $\xi = 26.5\sigma$, corresponds to the critical reduced density $\rho_b\sigma^3 = 0.3152$.

densities. The scaling function is always negative and a strong asymmetry is evident between the curves at density above and below ρ_c. For positive values of the scaling field h (i.e., $\rho > \rho_c$ in our case), the magnitude of the force becomes larger and larger and the peak is shifted towards small values of L/ξ.

B. Long wavelength analysis

Although the direct numerical evaluation of the critical Casimir scaling function predicted by this class of DFT is not conclusive, due to severe corrections to scaling, an accurate estimate of the asymptotic behavior can be obtained by a long wavelength (LW) analysis of the DFT equations. In fact, following Ref. [53] we note that

(1) the density profile $\rho(z)$ displays reflection symmetry about $z = \frac{L}{2}$, limiting the range of interest to $z \in [0, \frac{L}{2}]$;

(2) when the walls are far apart ($L \gg \sigma$), the difference between the density profile corresponding to a wall-to-wall distance L and its single-wall limit, reached for $L = \infty$, is significant only for $z \sim \frac{L}{2}$;

(3) as a consequence, the effective force per unit surface F_C (hence the Casimir scaling function) just depends on the long distance tail of the density profile, which is expected to be a slowly varying function of the coordinate z.

Therefore our WDA intrinsic free energy functional can be approximated by keeping only the lowest term in a gradient expansion about the bulk density ρ_b:

$$\frac{\beta\mathcal{F}[\rho_b + \delta n(z)]}{\Sigma} = L\varphi(\rho_b) + \int dz \left[\frac{b}{2}\left(\frac{d\delta n(z)}{dz}\right)^2 + \varphi(\rho_b + \delta n(z)) - \varphi(\rho_b)\right], \quad (33)$$

where $\varphi(\rho)$ is the free energy density in the bulk, times β. This expression coincides with the long wavelength limit of our WDA functional, the stiffness b being related to the range of the direct correlation function in the homogeneous system $c(r, \rho_b)$:

$$-\int d\boldsymbol{r}\, c(r;\rho_b) e^{i\boldsymbol{q}\cdot\boldsymbol{r}} \longrightarrow \frac{\partial^2\varphi(\rho_b)}{\partial\rho_b^2} + bq^2 + O(q^4). \quad (34)$$

In the presence of short range interactions, the direct correlation function is analytic in q^2 away from the critical point, where it displays a $q^{2-\eta}$ singularity. However, within our approximate closure of the HRT equations, the critical exponent $\eta = 0$ and analyticity is preserved also at criticality [22], keeping the stiffness b finite in the whole phase diagram. This implies that the long wavelength limit of the structure factor of the homogeneous fluid follows the Orstein-Zernike ansatz:

$$S(q) \sim \frac{S(0)}{1 + \xi^2 q^2} \quad (35)$$

with

$$\rho_b\, S(0) = \left[\frac{\partial^2\varphi(\rho)}{\partial\rho^2}\right]^{-1} \quad (36)$$

and $\xi^2 = \rho\, S(0)\, b$. Close to the critical point, the HRT bulk free energy density $\varphi(\rho)$ acquires a scaling form:

$$\varphi(\rho_c + \delta\rho) - \varphi(\rho_c) - \beta\mu(\rho_c)\delta\rho = t^{d\nu}\, a_{11}\, \Psi(b_1\, \delta\rho\, t^{-\beta}), \quad (37)$$

where ρ_c is the critical density and $\mu(\rho)$ is the chemical potential (the temperature dependence of these quantities is understood), while a_{11} and b_1 are nonuniversal metric factors and $t = (T - T_c)/T_c$ is the reduced temperature. In the following it will be convenient to express the universal quantities in terms of the scaling field $x = b_1\, \delta\rho\, t^{-\beta}$ instead of the previously defined variable y. Within our HRT closure, the critical exponents are $\delta = 5$, $\beta = 0.332$, $\nu = 0.664$ in $d = 3$, which agree within 10% with the accepted values. The metric factors appearing in the scaling function are implicitly defined by the requirement that $\Psi(x)$ has the following expansion at small x [57]:

$$\Psi(x) \longrightarrow \frac{x^2}{2!} + \frac{x^4}{4!} + O(x^6). \quad (38)$$

In Fig. 15 the asymptotic HRT scaling function $\Psi(x)$ is shown together with a parametrization of the exact result for the 3D Ising universality class. Although the two curves are indistinguishable on this scale, calculations at different reduced temperatures, also shown, suggest the presence of important corrections to scaling.

The minimization of the long wavelength functional (33) in slab geometry gives rise to a differential equation whose solution allows us to evaluate the asymptotic decay of the effective force between two hard walls in a critical fluid. The derivation, already detailed in Ref. [53] and not repeated here, provides a closed form for the critical Casimir scaling function in terms of two universal quantities: the bulk free energy scaling function $\Psi(x)$ and the universal amplitude ratio g_4^+. Defining the auxiliary quantity $\sigma(s,x)$ by the implicit

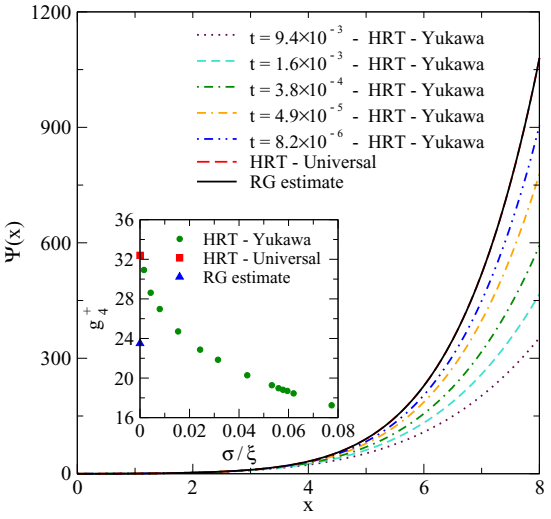

FIG. 15. Scaling function for the free energy $\Psi(x)$ as predicted by HRT compared with a parametrization of the exact result from Ref. [57] (black curve). The red line, showing the HRT asymptotic result, is identical to the exact result on the scale of the figure. A few rescaled free energies obtained from the integration of the HRT equations at different reduced temperatures are also shown. Inset: Universal amplitude ratio g_4^+ for a HCY fluid at the critical density as a function of the reduced inverse correlation length (green points). The usually accepted value [57] is shown by a blue triangle whereas the red square represents the asymptotic HRT value.

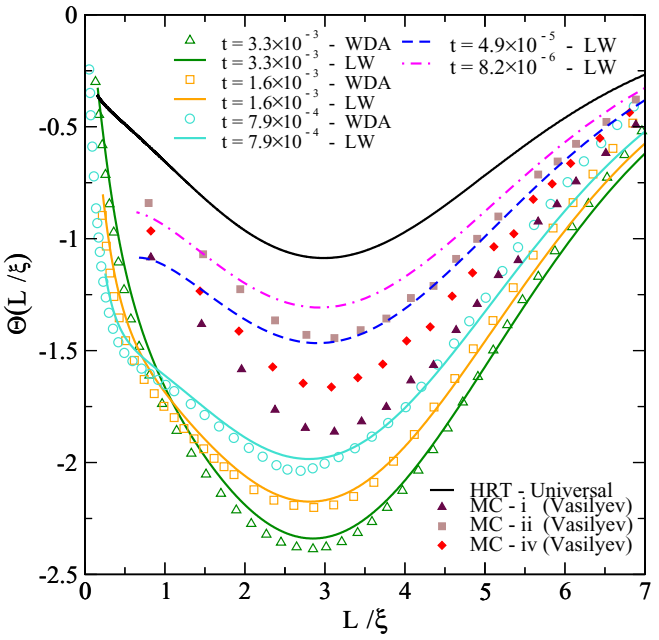

FIG. 16. Critical Casimir scaling function evaluated at different reduced temperatures. Points: Results from the direct minimization of the microscopic WDA functional. Lines: Results from the long wavelength analysis, starting from the universal quantities $\Psi(x)$ and g_4^+ evaluated at the same reduced temperature as the DFT calculation. Black line: Asymptotic limit of the critical Casimir scaling function. Points: Prediction of Θ from Monte Carlo simulations [48].

relations

$$\sigma(s,x) = -\Psi(x+u_0) + \Psi(x) + u_0\,\Psi'(x), \tag{39}$$

$$s = \int_{u_0}^{\infty} \frac{\sqrt{2}\,du}{\sqrt{\sigma(s,x) + \Psi(x+u) - \Psi(x) - u\,\Psi'(x)}}, \tag{40}$$

the critical Casimir scaling function in three dimensions is given by

$$\Theta(s,x) = \frac{s^3}{g_4^+}\sigma(s,x). \tag{41}$$

The universal amplitude ratio g_4^+ is expressed in terms of the nonuniversal metric factors previously introduced as

$$g_4^+ = b_1^3\sqrt{a_{11}b^{-3}}. \tag{42}$$

Again, the evaluation of g_4^+ from the HRT equations displays severe correction to scaling in a HCY fluid, as shown in the inset of Fig. 15. More importantly, the usually quoted "exact" value [57] $g_4^+ \sim 23.6$ turns out to differ significantly from the HRT prediction $g_4^+ \sim 32.4$.

The asymptotic study of the DFT equations allows us to extract the critical Casimir scaling function just from bulk quantities via Eqs. (39)–(41). It is then instructive to contrast these predictions with the outcome of the direct minimization of the HRT functional, already shown in Fig. 13. Such a comparison can be found in Fig. 16, where the scaling functions obtained from the microscopic DFT at a few reduced temperatures t in the critical region are shown to agree remarkably well with the predictions of the long wavelength analysis, provided both the scaling function for the free energy $\Psi(x)$ and the universal amplitude ratio g_4^+ are consistently evaluated at the same reduced temperature t.

The presence of strong corrections to scaling in both $\Psi(x)$ and g_4^+, already highlighted, induces strong preasymptotic effects in the critical Casimir scaling function which, at reduced temperatures lower than 10^{-3}, is still quite far from its asymptotic limit. The main effect is due to the growth of the amplitude ratio, which, as shown in Fig. 15, appears to reach its universal value only extremely close to the critical point, according to the prediction of HRT for the model of critical fluid investigated here. We remark that, due to the already quoted difference between the HRT estimate of the universal amplitude ratio g_4^+ and the value obtained via series expansions, the critical Casimir scaling function predicted by our DFT significantly differs from the one obtained in MC simulations, as can be seen in Fig. 16.

V. CONCLUSIONS AND PERSPECTIVES

We presented a density functional, based on the weighted density paradigm, able to describe classical inhomogeneous fluids in a large portion of their phase diagram, critical point included. This is the first attempt to describe the effects of correlations induced by attractive interactions in confined fluids. The theory is based on the description of the uniform system provided by the hierarchical reference theory, one of the few liquid state approaches able to cope with long range density fluctuations. This technique, applied to the evaluation of the effective interaction between two hard walls in a fluid, allowed for the investigation of the crossover between a depletion-like mechanism at high temperatures and the critical

Casimir effect emerging near the critical point. Our method does not rely on a long wavelength approximation and provides a complete picture of the solvent-mediated force for any wall separation, displaying the presence of important nonuniversal contributions in the effective interaction at short distances, even in the critical region. We believe that this DFT will be useful in investigating other correlated systems, when density fluctuations are expected to play an important role.

We showed that, at large separations, the solvent-mediated force per unit surface between the walls decays exponentially on the scale of the correlation length in the whole portion of the phase diagram to the left of the Fisher-Widom line. Such a behavior cannot be considered as a signature of the onset of critical Casimir effect: only the product between the *amplitude* of the long range exponential tail and the cube of the correlation length is a genuine universal quantity.

Our microscopic approach allows for the determination of the universal quantities characterizing the critical Casimir effect, namely the scaling function $\Theta(s, y)$, both along the critical isochore ($y = 0$) and in the off-critical regime. Strong corrections to scaling have been observed in the HCY fluid we investigated: The universal features appear to emerge only in a narrow neighborhood of the critical point, at least in the model we examined. It would be useful to compare this prediction with numerical simulations for the HCY fluid model as well as with theoretical investigations of other systems, like the Ising model, where the correction to scaling may be weaker. These studies will hopefully clarify the origin of the discrepancy between the HRT estimate of the universal amplitude ratio g_4^+ and the commonly accepted value.

The approach presented in this work allows for further improvements. In our density functional, the ideal gas term and the Hartree contribution to the internal energy have been treated exactly, while the remaining entropy-correlation term has been approximated by use of a weighted density trick. The next step will be to treat the hard sphere term by the fundamental measure theory, known to be very accurate in dealing with excluded volume effects, limiting the weighted density contribution only for the residual correlation term. This adjustment is expected to increase the accuracy of the theory at high density, without however modifying the description of the universal properties of the critical Casimir effect.

In this first application we just considered a planar geometry, whose implications for the phenomenon of colloidal aggregation depend upon further assumptions, namely the Derjaguin approximation, which however turns out to be rather inaccurate when the two external bodies are not very close. A natural further step will be to perform the functional minimization in cylindrical geometry, appropriate for dealing with two spherical particles thereby avoiding any wall-to-sphere mapping.

Finally, a very interesting application of this formalism will be the investigation of subcritical temperatures, where wetting phenomena are expected close to the first order transition boundary. The hierarchical reference theory of fluids provides a consistent description of the full liquid-vapor transition line and then it appears to be the natural starting point for the development of a microscopic theory, beyond mean field, for the study of phase coexistence near a wall.

[1] S. Asakura and F. Oosawa, J. Chem. Phys. **22**, 1255 (1954).
[2] S. Asakura and F. Oosawa, J. Polym. Sci. **33**, 183 (1958).
[3] R. Roth, R. Evans, and S. Dietrich, Phys. Rev. E **62**, 5360 (2000).
[4] D. J. Ashton, N. B. Wilding, R. Roth, and R. Evans, Phys. Rev. E **84**, 061136 (2011).
[5] A. A. Louis, E. Allahyarov, H. Lowen, and R. Roth, Phys. Rev. E **65**, 061407 (2002).
[6] M. E. Fisher and P. G. de Gennes, C. R. Seances Acad. Sci., Ser. B **287**, 207 (1978).
[7] C. Hertlein, L. Helden, A. Gambassi, S. Dietrich, and C. Bechinger, Nature (London) **451**, 172 (2008).
[8] N. Gnan, E. Zaccarelli, P. Tartaglia, and F. Sciortino, Soft Matter **8**, 1991 (2012).
[9] N. Gnan, E. Zaccarelli, and F. Sciortino, J. Chem. Phys. **137**, 084903 (2012).
[10] S. Buzzaccaro, J. Colombo, A. Parola, and R. Piazza, Phys. Rev. Lett. **105**, 198301 (2010).
[11] S. Buzzaccaro, R. Piazza, J. Colombo, and A. Parola, J. Chem. Phys. **132**, 124902 (2010).
[12] H. Löwen, J. Phys.: Condens. Matter **14**, 11897 (2002).
[13] D. Henderson, *Fundamentals of Inhomogeneous Fluids* (Marcel Dekker, New York, 1992).
[14] J.-P. Hansen and I. R. McDonald, *Theory of Simple Liquids* (Academic Press, London, 2013), 4th ed.
[15] N. D. Mermin, Phys. Rev. **137**, A1441 (1965).
[16] P. Hohenberg and W. Kohn, Phys. Rev. **136**, B864 (1964).
[17] Y. Rosenfeld, Phys. Rev. Lett. **63**, 980 (1989).
[18] R. Roth, J. Phys.: Condens. Matter **22**, 063102 (2010).
[19] P. Tarazona, Phys. Rev. A **31**, 2672 (1985).
[20] W. A. Curtin and N. W. Ashcroft, Phys. Rev. A **32**, 2909 (1985).
[21] A. Parola and L. Reatto, Adv. Phys. **44**, 211 (1995).
[22] A. Parola, D. Pini, and L. Reatto, Mol. Phys. **107**, 503 (2009).
[23] R. Leidl and H. Wagner, J. Chem. Phys. **98**, 4142 (1993).
[24] J. Henderson, Mol. Phys. **59**, 89 (1986).
[25] R. Evans and A. O. Parry, J. Phys.: Condens. Matter **2**, SA15 (1990).
[26] F. van Swol and J. R. Henderson, Phys. Rev. A **40**, 2567 (1989).
[27] R. Groot, N. Faber, and J. van der Eerden, Mol. Phys. **62**, 861 (1987).
[28] R. Roth, R. Evans, A. Lang, and G. Kahl, J. Phys.: Condens. Matter **14**, 12063 (2002).
[29] E. Garnett, L. Mier-Y-Terán, and F. D. Río, Mol. Phys. **97**, 597 (1999).
[30] W. Olivares-Rivas, L. Degrève, D. Henderson, and J. Quintana, J. Chem. Phys. **106**, 8160 (1997).
[31] F.-Q. You, Y.-X. Yu, and G.-H. Gao, J. Phys. Chem. B **109**, 3512 (2005).
[32] S. Karanikas, J. Dzubiella, A. Moncho-Jordá, and A. A. Louis, J. Chem. Phys. **128**, 204704 (2008).
[33] M. Wertheim, L. Blum, and D. Bratko, in *Micellar Solutions and Microemulsions*, edited by S.-H. Chen and R. Rajagopalan (Springer, New York, 1990), pp. 99–110.

[34] R. Evans, J. Henderson, D. Hoyle, A. Parry, and Z. Sabeur, Mol. Phys. **80**, 755 (1993).
[35] W. E. Brown, Mol. Phys. **88**, 579 (1996).
[36] A. Gambassi, A. Maciołek, C. Hertlein, U. Nellen, L. Helden, C. Bechinger, and S. Dietrich, Phys. Rev. E **80**, 061143 (2009).
[37] R. Evans and J. Stecki, Phys. Rev. B **49**, 8842 (1994).
[38] B. Derjaguin, Kolloid-Zeitschrift **69**, 155 (1934).
[39] B. Götzelmann, R. Evans, and S. Dietrich, Phys. Rev. E **57**, 6785 (1998).
[40] M. G. Noro and D. Frenkel, J. Chem. Phys. **113**, 2941 (2000).
[41] G. A. Vliegenthart and H. N. W. Lekkerkerker, J. Chem. Phys. **112**, 5364 (2000).
[42] D. Pini, G. Stell, and N. B. Wilding, Mol. Phys. **95**, 483 (1998).
[43] I. Brankov, D. M. Danchev, N. S. Tonchev, and J. G. Brankov, *Theory of Critical Phenomena in Finite-Size Systems: Scaling and Quantum Effects* (World Scientific, Singapore, 2000).
[44] M. N. Barber, in *Phase Transitions and Critical Phenomena*, edited by C. Domb, M. Green, and J. Lebowitz (Academic Press, New York, 1983), Vol. 8, pp. 145–266.
[45] M. Fukuto, Y. F. Yano, and P. S. Pershan, Phys. Rev. Lett. **94**, 135702 (2005).
[46] S. Rafai, D. Bonn, and J. Meunier, Phys. A (Amsterdam, Neth.) **386**, 31 (2007).
[47] O. Vasilyev, A. Gambassi, A. Maciolek, and S. Dietrich, Europhys. Lett. **80**, 60009 (2007).
[48] O. Vasilyev, A. Gambassi, A. Maciolek, and S. Dietrich, Phys. Rev. E **79**, 041142 (2009).
[49] O. Vasilyev, A. Maciołek, and S. Dietrich, Phys. Rev. E **84**, 041605 (2011).
[50] M. Krech, Phys. Rev. E **56**, 1642 (1997).
[51] Z. Borjan and P. J. Upton, Phys. Rev. Lett. **101**, 125702 (2008).
[52] P. J. Upton and Z. Borjan, Phys. Rev. B **88**, 155418 (2013).
[53] R. Piazza, S. Buzzaccaro, A. Parola, and J. Colombo, J. Phys.: Condens. Matter **23**, 194114 (2011).
[54] F. Schlesener, A. Hanke, and S. Dietrich, J. Stat. Phys. **110**, 981 (2003).
[55] T. F. Mohry, S. Kondrat, A. Maciolek, and S. Dietrich, Soft Matter **10**, 5510 (2014).
[56] O. A. Vasilyev and S. Dietrich, Europhys. Lett. **104**, 60002 (2013).
[57] A. Pelissetto and E. Vicari, Phys. Rep. **368**, 549 (2002).
[58] It is precisely an Abel differential equation of the second kind, which, in a range of densities, has no solutions satisfying the physical boundary conditions.